Research Article | Vol. 28, No. 26 / 21 December 2020 / Optics Express 39827
Optics EXPRESS

Third-order Riemann pulses in optical fibers

DOMENICO BONGIOVANNI,[1,2] BENJAMIN WETZEL,[3] ZHILI LI,[1] YI HU,[1] STEFAN WABNITZ,[4,5] ROBERTO MORANDOTTI,[2,6,8] AND ZHIGANG CHEN[1,7,9]

[1]TEDA Applied Physics Institute and School of Physics, Nankai University, Tianjin 300457, China
[2]INRS-EMT, 1650 Blvd. Lionel-Boulet, Varennes, QC J3X 1S2, Canada
[3]XLIM Research Institute, CNRS UMR 7252, Université de Limoges, Limoges 87060, France
[4]DIET, Sapienza University of Rome, Via Eudossiana 18, Rome 00184, Italy
[5]Physics Department, Novosibirsk State University, 1 Pirogova Street, Novosibirsk 630090, Russia
[6]Institute of Fundamental and Frontier Sciences, University of Electronic Science and Technology of China, Chengdu 610054, China
[7]Department of Physics & Astronomy, San Francisco State University, San Francisco, CA 94132, USA
[8]morandotti@emt.inrs.ca
[9]zgchen@nankai.edu.cn

Abstract: We introduce the concept of third-order Riemann pulses in nonlinear optical fibers. These pulses are generated when properly tailored input pulses propagate through optical fibers in the presence of higher-order dispersion and Kerr nonlinearity. The local propagation speed of these optical wave packets is governed by their local amplitude, according to a rule that remains unchanged during propagation. Analytical and numerical results exhibit a good agreement, showing controllable pulse steepening and subsequent shock wave formation. Specifically, we found that the pulse steepening dynamic is predominantly determined by the action of higher-order dispersion, while the contribution of group velocity dispersion is merely associated with a shift of the shock formation time relative to the comoving frame of the pulse evolution. Unlike standard Riemann waves, which exclusively exist within the strong self-defocusing regime of the nonlinear Schrödinger equation, such third-order Riemann pulses can be generated under both anomalous and normal dispersion conditions. In addition, we show that the third-order Riemann pulse dynamics can be judiciously controlled by a phase chirping parameter directly included in the initial chirp profile of the pulse.

1. Introduction

Simple Riemann waves (RWs) are implicit solutions of the inviscid Burgers' equation (IBE), that lies at the basis of fluid dynamics. These waves are of fundamental importance in studying shock wave phenomena occurring not only in hydrodynamics but also in numerous other physical systems [1–12]. Interest in RWs arises from the main role played by the IBE, a paradigm nonlinear partial differential equation which is used to model nonlinear and turbulent systems of various complexity, spanning dynamics encountered in e.g. astrophysics [13], Bose-Einstein condensation [14], financial markets [15] and traffic flows [16,17]. Such an equation can be derived from the Euler momentum equation in the absence of pressure gradient and external forces [18], but it can also be obtained, under appropriate conditions, from the nonlinear Schrödinger equation (NLSE). The latter well-established model is largely used to describe, for example, the evolution of electromagnetic pulses in nonlinear optics [19,20], plasmas [21], and ocean wave dynamics [22]. In particular, over the last few years, the NSLE analogy between optics and hydrodynamics has increasingly favored the use of nonlinear optical waveguides (such as optical fibers) as a testbench to investigate and observe nontrivial water wave phenomena, as well as for establishing intriguing connections between these two physical domains [23]. Driven by the initial observation of optical rogue waves [24], research efforts in optics have been primarily

#411736 https://doi.org/10.1364/OE.411736
Journal © 2020 Received 6 Oct 2020; revised 16 Nov 2020; accepted 17 Nov 2020; published 16 Dec 2020

Optics EXPRESS

conducted in the self-focusing regime of the NLSE, where similarities with extreme events formation in deep-water wave hydrodynamics have been extensively studied [25–28], especially focusing on the process of modulation instability and associated nonlinear optical breather and soliton solutions [24,29–31].

In parallel, the NLSE self-defocusing regime was also widely explored. In this case, optical studies mainly focused on mimicking hydrodynamics phenomena described by the nonlinear shallow water equation (NSWE) [32,33]. Indeed, when the nonlinearity is predominant over dispersive effects (i.e., the strong defocusing condition), the NLSE can be reduced to its semiclassical NSWE approximation. Compared to hydrodynamics, the optical envelope amplitude plays the role of the water height and the pulse chirp (i.e. the derivative of the phase, or instantaneous frequency) plays the role of the wave velocity [34–37]. In the framework of nonlinear optical fibers, NSWE analogies have been the focal point of different studies, such as the formation of optical tsunamis [38] and undular bores [39], the observation of photonic dam-breaks [40,41], as well as of hydrodynamic optical soliton tunneling [42]. Among all available analytical solutions of the NSWE [34], RWs have attracted a growing interest in the framework of the above-mentioned link with shock wave phenomena. Recently, experimental observations of random RWs in the context of an integrable turbulence [9], as well as the signature and control of simple RWs in both temporal [7] and spatial [10] domains, have been reported. In general, the NSWE consists of two coupled nonlinear partial differential equations, which are determined by two Riemann invariant solutions. For simple RWs, the NSWE system reduces to one IBE, as the envelope amplitude is proportional to the phase chirp, and this proportionality relationship remains intact during nonlinear evolution. Nevertheless, higher-order dispersive effects in optical fibers tend to prove detrimental to a Riemann wave evolution. For instance, they lead (under certain conditions) to a continuous compression of the pulse envelope, and the formation of extreme events [38]. To preserve the typical Riemann dynamics, low values of high-order dispersion coefficients are preferable, as it was done for the observation of Gaussian Riemann pulses in a highly nonlinear fiber (HNLF) [7]. However, a strong defocusing condition is typically reached for short pulses featuring high power (and thus usually exhibiting a large bandwidth), in a wavelength range where the dispersion is low (i.e., generally close to the fiber zero-dispersion wavelength (ZDW)). In this regime, the ability to neglect the effects associated with higher-order dispersion terms can therefore become questionable, and one may wonder whether similar RW solutions can still retain analogous physical properties.

In this work, we introduce a new class of optical RWs, namely third-order Riemann pulses (TRPs), and study these optical wave-packets in the context of nonlinear optical fiber propagation. The dynamics of TRPs originate from the interplay between higher-order dispersion effects and Kerr nonlinearity. Their nonlinear evolutions exhibit progressive steepening with constant peak intensity and subsequent shock wave formation, with similar general dynamics yet different characteristics and behaviors when compared with previously studied standard RWs. Guided by our theoretical analysis, we also perform numerical studies demonstrating the formation of TRPs by judiciously shaping an initial optical pulse before its injection into the fiber. Here, TRPs are numerically investigated under different propagation conditions, and their properties and differences with respect to RWs are discussed in detail. Unlike standard RWs, TRPs can be generated even within anomalous dispersion propagation, and therefore can exist under the self-focusing regime of the NLSE. Finally, we highlight a way to approximately control the TRPs, where the shock point can be tuned by acting appropriately on a phase term imprinted onto the initial optical pulse, without modifying the physical parameters of the fiber system.

2. Theory

The analysis starts from the generalized nonlinear Schrödinger equation (GNLSE), describing pulse propagation in an optical fiber under the action of the Kerr nonlinearity and the mutual

Optics EXPRESS

influence of both second- and third-order dispersions terms (SOD and TOD, respectively), expressed as [18]:

$$i\frac{\partial E}{\partial z} - \frac{\beta_2}{2}\frac{\partial^2 E}{\partial t^2} - \frac{i\beta_3}{6}\frac{\partial^3 E}{\partial t^3} + \gamma|E|^2 E = 0. \tag{1}$$

In Eq. (1), $E(t,z)$ represents an optical pulse envelope, where t is the time coordinate in the comoving frame of the pulse, traveling at the carrier frequency group velocity, and z is the propagation distance. The parameters β_2 and β_3 are the SOD and TOD group velocity dispersion (GVD) coefficients of the fiber, respectively. $\gamma = k_0 n_2$ is the nonlinear Kerr coefficient, with k_0 and n_2 denoting the vacuum wavenumber and the nonlinear refractive index, respectively. Note that for our analysis, the GNLSE does not explicitly include Raman scattering effects or linear losses. To provide a more general analysis, Eq. (1) is first reformulated in a dimensionless coordinate system, yielding:

$$i\frac{\partial A}{\partial Z} - \frac{\ddot{\beta}^2}{2}\frac{\partial^2 A}{\partial T^2} - \frac{i\bar{\beta}^3}{6}\frac{\partial^3 A}{\partial T^3} + |A|^2 A = 0, \tag{2}$$

where, $A(T,Z) = E(T,Z)/\sqrt{P_0}$ is the normalized electric field envelope, $T = t/T_0$, and $Z = z/L_{\mathrm{NL}}$, are the dimensionless temporal and longitudinal propagation coordinates, while $\ddot{\beta}^2 = \beta_2/(\gamma P_0 T_0^2)$ and $\bar{\beta}^3 = \beta_3/(\gamma P_0 T_0^3)$ correspond to the dimensionless SOD and TOD terms, respectively. $L_D = T_0^2/|\beta_2|$, $L'_D = T_0^3/|\beta_3|$ and $L_{NL} = (\gamma P_0)^{-1}$ denote the corresponding SOD/TOD dispersion and nonlinear lengths. Furthermore, to quantify the effective role of the optical pulse evolution played by both SOD and TOD, we also define $M = L'_D/L_D = T_0|\beta_2/\beta_3|$. The normalization of Eq. (2) is carried out by scaling the pulse duration by T_0, and the peak power by P_0. A way to find arbitrary solutions to Eq. (2) is to express the dimensionless pulse envelope in a polar form, by means of the Madelung transformation:

$$A(T,Z) = |A(T,Z)| \exp\left[-\frac{i}{\kappa}\int_{-\infty}^{T} u(T',Z)\, dT'\right], \tag{3}$$

with $u(T,Z)$ a real function, and κ a real-valued coefficient. When considering the pure NLSE case (i.e. where β_3 is null), the parameter κ can be readily obtained from the normalisation of the NLSE in terms of the caracteristic nonlinear length L_{NL} and dispersion length L_D of the system, so that $\kappa = \pm|\ddot{\beta}|$ [38]. Here however, we consider the predominant dispersive contribution of TOD (provided by β_3) in the GNLSE, and define κ as directly related to the ratio between the nonlinear length L_{NL} and the third order dispersion length L'_D, yielding $\kappa = \pm|\bar{\beta}|$. When considering the strongly nonlinear regime, where $L'_D >> L_{NL}$, the condition $\kappa << 1$ is satisfied, and high-order derivatives with respect to the time T can be neglected (for reasonably smooth pulse profiles). In such conditions, and similar to the case of a pure NLSE, Eq. (2) can be thus reduced to a semiclassical approximation of the GNLSE, resembling the nonlinear shallow water equation (NSWE) model [7,22,37]:

$$\begin{aligned} &\tfrac{\partial|A|}{\partial Z'} + \left(\tilde{\beta} + \tfrac{u}{2}\right) u \tfrac{\partial|A|}{\partial T} + \left(\tilde{\beta} + u\right)\tfrac{\partial u}{\partial T} = 0 \\ &\tfrac{\partial u}{\partial Z'} + \left(\tilde{\beta} + \tfrac{u}{2}\right) u \tfrac{\partial u}{\partial T} + \tfrac{\partial|A|}{\partial T} = 0 \end{aligned}, \tag{4}$$

where $Z' = \kappa Z$, $\tilde{\beta} = \ddot{\beta}^2/\bar{\beta}^2$. The NSWE-like system in Eq. (4) is composed of two coupled partial differential equations, and it admits two Riemann invariant solutions. Among them, a specific solution, known as simple RW (or just RW), can be found by setting one of these Riemann invariants to a null value, thus reducing the NSWE-like system to a single nonlinear wave equation, the IBE. In the absence of TOD, simple RW solutions of the NLSE have been introduced [4] and demonstrated [7,10] in both the spatial and the temporal domains as a solution of the IBE.

Optics EXPRESS

Specifically, these standard RWs can only be generated under the strong self-defocusing regime of the NLSE, where the Kerr nonlinearity greatly overcomes the magnitude of either diffraction or dispersion effect. For Riemann pulses in nonlinear fibers, the latter condition reduces to the case of considering only low normal dispersion and a dominant Kerr nonlinearity [4]. Nevertheless, in a real-world optical fiber, standard Riemann pulses represent an ideal limit case. However, they are difficult to achieve due to the undesired presence of higher-order dispersion effects, which may significantly affect their propagation. Therefore, it is necessary to determine the range of applicability of the RW solution, in situations where the GNLSE system can be well approximated by its NSWE reduction. As an example, the value of M calculated from the pulse and fiber parameters reported in Ref. [7] is equal to 96.87, while κ is equal to approximately 0.104 (with $\kappa = \pm|\ddot{\beta}|$ in the framework of a standard RW solution of the NLSE). In order to investigate the effective influence of TOD on ordinary RW dynamics in this particular case, we performed numerical simulations of RW pulse evolution by considering different values of M, while keeping the value of κ constant (i.e., a condition that is achieved by only varying the TOD coefficient). The relative variation of the pulse peak intensity at the shock distance was used for a comparison with the ideal case (i.e., without TOD). We found that for $M>100$, the discrepancy on the peak intensity variation remains under 3 %, thus making the effect of β_3 small enough to be considered negligible in this range. However, for values $M<100$, TOD starts to significantly affect the evolution of RWs, so that the NLSE approximation (i.e., neglecting TOD in the GNLSE) is no longer fully acceptable to describe RW propagation dynamics. Exploring the existence of simple RW solutions, even for the GNLSE including higher-order dispersive terms, is not only useful because its description via a NSWE-like system is significantly simplified, but it is also advantageous as it allows for employing the well-known experimental methods already implemented for the observation and control of standard RWs [7,9,39]. In this framework, we consider the pulse envelope described in Eq. (3) and assume the chirp profile - or instantaneous phase derivative - $u(T,Z)$ to be:

$$u(T,Z) = (3|A(T,Z)| + a)^{2/3} - \frac{\ddot{\beta}^2}{\bar{\beta}^2}, \tag{5}$$

where the constant-coefficient a is the phase-chirping control parameter for the RW and $\kappa = \bar{\beta} << 1$. By substituting the chirp profile into Eq. (4), the NSWE-like system can be reduced to a nonlinear shock wave equation, reading as:

$$\frac{\partial|A|}{\partial Z} + \left(\frac{5\bar{\beta}}{6}(3|A| \ + a)^{4/3} - \frac{a\bar{\beta}}{3}(3|A| + a)^{1/3} - \frac{\ddot{\beta}^2}{2\bar{\beta}}\right)\frac{\partial|A|}{\partial T} = 0. \tag{6}$$

Remarkably, pulse propagation dynamics in nonlinear optical fibers, which is described by the GNLSE in Eq. (1), can still be efficiently modeled in terms of a nonlinear Riemann wave, whose implicit form is:

$$|A_{TRP}(T,Z)| = \left|A_{TRP}\left(T - \left(\frac{5\bar{\beta}}{6}(3\,|A_{TRP}(T,Z)| \ + a)^{4/3} - \frac{a\bar{\beta}}{3}(3\,|A_{TRP}(T,Z)| + a)^{1/3} - \frac{\ddot{\beta}^2}{2\bar{\beta}}\right)Z\right)\right|, \tag{7}$$

where $A_{TRP}(T) = A(T,0)$ is the amplitude envelope at the onset of the propagation. Equation (7) represents one of the key results of this study, illustrating how the GNLSE dynamics can, under certain conditions, be approximated by a nonlinear Riemann pulse evolution. Corresponding characteristic curves for Eq. (6) are expressed by the following parametric representation:

$$T(T_0,Z) = T_0 - \frac{\ddot{\beta}^2}{2\bar{\beta}}Z + \left(\frac{5\bar{\beta}}{6}(3|A_{TRP}(T_0,0)| \ + a)^{4/3} - \frac{a\bar{\beta}}{3}(3|A_{TRP}(T_0,0)| + a)^{1/3}\right)Z\,, \tag{8}$$

where T_0 is an arbitrary point in the temporal axis at the fiber input end (i.e., for $Z = 0$). The characteristic lines start to cross in the $T - Z$ plane at the shock point (T_{SC}, Z_{SC}), where the

Optics EXPRESS

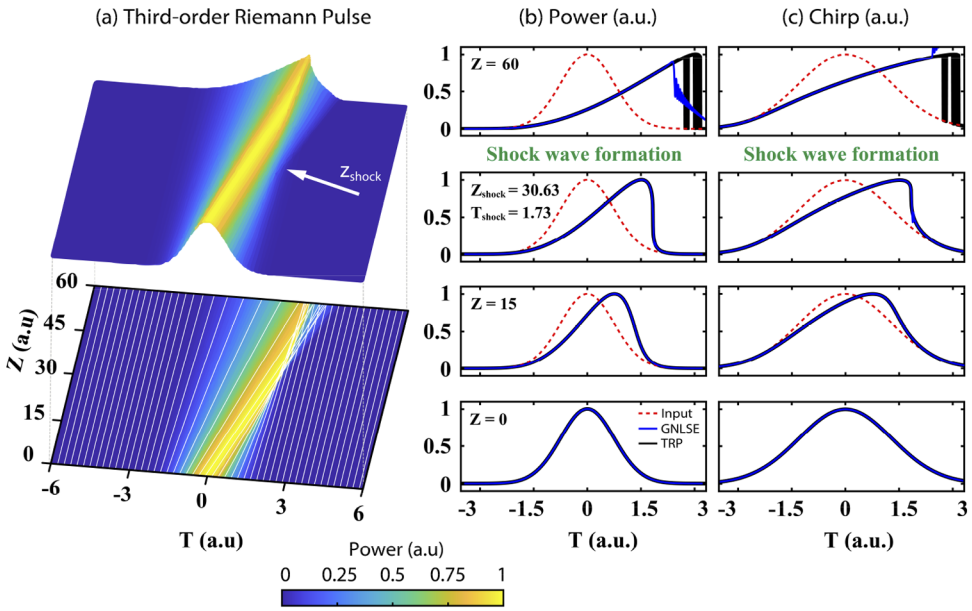

Fig. 1. (a) Three-dimensional (3D) dimensionless longitudinal intensity distribution of GNLSE simulations ($\bar{\beta} = 0.013$) used to model the evolution of a TRP in a nonlinear optical fiber at the ZDW (top). The projected pulse intensity (bottom) is compared with the characteristic lines obtained analytically from theory (white solid lines), showing shock formation at $Z = 30.63$ and T=1.73. (b-c) Temporal profiles of (b) intensity and (c) chirp are shown at selected distances, comparing IBE predictions (black solid lines) with GNLSE simulations (blue solid lines). Dashed red lines highlight the input profiles for both temporal intensity and chirp profiles.

tangent slope to the wave amplitude tends to infinity. The coordinates of this point can be readily calculated by the relations $T_{SC} = T(T_{0SC}, Z_{SC})$ and $Z_{SC} = -[\partial \mathrm{G}(T_{0SC}, 0)/\partial T]^{-1}$ where $\mathrm{G}(T, 0) = 5\bar{\beta}/\,6\,(\,3\,|A_{TRP}(T_0, 0)|\,+\,a)^{4/3} - \,a\,\bar{\beta}/\,3\,(\,3\,|A_{TRP}(T_0, 0)|\,+\,a)^{1/3}$, with T_{0SC} being the value corresponding to $min[(-\partial|A_{TRP}(T,0)|/\partial T)^{-1}]$. Next, in order to demonstrate the validity of the aforementioned approach, we perform a numerical study of TRPs propagating under different conditions and parameters. Simulations are carried out via a split-step Fourier transform method applied to Eq. (1). The input profile of the TRP is determined via Eq. (3), while the chirp profile is numerically calculated via Eq. (5).

3. Third-order Riemann pulses at the zero-dispersion wavelength

At first, let us examine the nonlinear propagation of optical TRPs at the ZDW of the fiber. For simplicity, the control coefficient a is not taken into consideration at this stage, but its contribution will be discussed in the next sections. Under these conditions (i.e. $a = 0$ and $\ddot{\beta} = 0$), the pulse evolution in the frame of the GNLSE is only impacted by a pure TOD (the SOD is vanishing), and can be modelled by means of the "standard" IBE:

$$\frac{\partial P}{\partial Z} + P\frac{\partial P}{\partial T} = 0, \tag{9}$$

where $P(T, Z) = 2.5\bar{\beta}\sqrt[3]{3|A_{TRP}(T, Z)|^4}$. Therefore, Eq. (7) takes the form of standard RWs [4]. As an example, Fig. 1(a) illustrates the normalized longitudinal intensity distributions simulated by solving the GNLSE, obtained by nonlinearly propagating a Gaussian TRP at the ZDW of an

Optics EXPRESS

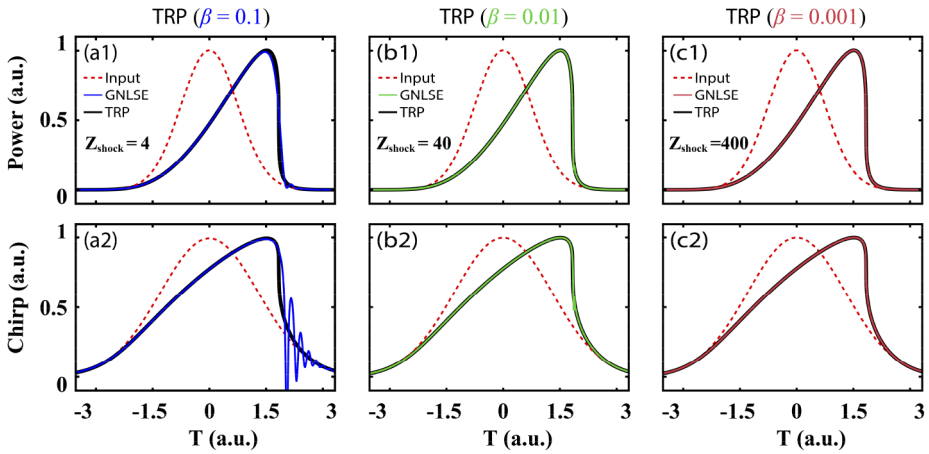

Fig. 2. Comparison between dimensionless GNLSE simulations and the corresponding theoretical predictions (black solid lines) of Gaussian TRPs for different values of $\bar{\beta}$. (a1-a3). Normalized temporal intensity profiles extracted at the shock distances for $\bar{\beta}$ equal to (a1) 0.1, (b1) 0.01, and (c1) 0.001. (a2-c2) Corresponding chirp profiles. Red dashed lines in the upper and lower panels show, respectively, the temporal intensity and chirp profiles at the onset of propagation.

optical fiber (i.e. under the exclusive influence of a positive TOD). Without loss of generality, the normalized coefficient $\bar{\beta}$ used in simulations is 0.013, which satisfies the conditions for the NSWE approximation (κ<<1). A Gaussian TRP is considered at the onset of the propagation (i.e. $|A_{TRP}(T,Z=0)| = \exp(-T^2/2)$). The instantaneous frequency of a transformed-limited Gaussian pulse is suitably adjusted so that the temporal chirp and amplitude profiles are not proportional, in contrast to the standard case [38], but they instead follow the relationship given by Eq. (5). Both the input intensity and chirp profiles are shown in Figs. 1(b) and (c), marked by dashed red lines. Looking at the three-dimensional map in the upper panel of Fig. 1(a), we can observe that the intensity profile of the initial Gaussian TRP experiences a progressive steepening of its trailing edge during propagation. Subsequently, the formation of a gradient catastrophe (or shock wave formation), where the envelope derivative tends to infinity, is observed. The assumption $\bar{\beta}$ = 0.013 leads to a shock formation that takes place at the dimensionless propagation distance and time of Z = 30.63 and T = 1.73, respectively - see the 2nd panels in Figs. 1(b) and (c). Here, the peak intensity of the TRP remains almost constant at the early stage of the nonlinear evolution (i.e., up to the gradient catastrophe), and starts decaying significantly afterward. A quantitative confirmation of these dynamics can be obtained from the analytical calculation of the characteristic lines from the IBE in Eq. (9). The characteristic line representation is useful to provide a parametric description of the unidirectional energy flow that is distinctive of RWs [34]. Overlapping the projection of the simulated intensity evolution for the GNLSE solution with the characteristic lines from the IBE (see white lines in Fig. 1(a)), one can notice an excellent agreement, thus illustrating the validity of the analytical IBE description until the shock is formed. This feature is also shown in Fig. 1(b) and (c), where we extracted both temporal intensity and chirp profiles at selected distances from GNLSE simulations and IBE theoretical predictions. Numerical profiles match very well with IBE profiles up to the shock distance, after which the IBE model is not suitable anymore to describe the GNLSE system. Since the characteristic lines start to intersect at the shock distance, theoretically giving rise to a multi-valued solution, the IBE cannot be used to approximate the nonlinear evolution in fibers after this point. It is worth noticing that the nonlinear steepening dynamics associated with TRPs rely on the $\bar{\beta}$ parameter, thus it is induced by the simultaneous action of nonlinearity and TOD on a suitably pre-shaped input pulse. From a physical viewpoint, the behavior of TRPs is

Optics EXPRESS

different from the well-known self-steepening phenomenon in optical fibers, originating from the frequency dependence of the nonlinearity and in the absence of group velocity dispersion [19]. The main role played by TOD on the pulse steepening process represents the different characteristic of TRPs when compared with standard RWs, where the second-order dispersion (along with the nonlinearity) is involved in the steepening process. More importantly, unlike the standard Riemann pulses where the pulse chirp is a scaled replica of the amplitude [38], in TRPs this proportionality relationship does not apply anymore. In fact, for TRPs the pulse chirp and amplitude profiles are linked by the nonlinear function of Eq. (5). Here, the choice of the parameter $\bar{\beta}$ is not only central to achieve high-quality TRPs, but it also enables a versatile and controllable shock wave formation. To prove this assertion, we compared in Fig. 2 the intensity and chirp profiles corresponding to Gaussian TRPs obtained when considering three different values of $\bar{\beta}$. Each plot is selected from GNLSE simulations at the shock distance and compared with analytical predictions obtained from the IBE in Eq. (9). For values of $\bar{\beta}$ higher than 0.1, the GNLSE simulations present discrepancies compared with IBE theory (especially in the pulse trailing edge) even though a constant peak intensity evolution is still noticeable [Fig. 2(a1)]. This can be explained by observing the associated chirp profile in Fig. 2(a2): the pulse does not reach a quasi-vertical front but, instead, its chirp profile starts developing oscillations, a typical signature of shock wave formation and regularization [4,8]. As the value of $\bar{\beta}$ decreases, the amplitude of these oscillations significantly reduces, and the agreement between GNLSE profiles and TRPs analytical predictions drastically improves (see Figs. 2(b1) and 2(b2)), until being almost indistinguishable for values of $\bar{\beta}$ lower than 0.001 (see Figs. 2(c1) and 2(c2)). We can assert that the values of $\bar{\beta}$ smaller than 0.1 are desirable for generating TRPs with satisfactory quality and fidelity. It is noteworthy that the numerical results in Fig. 2 highlight the capability to tune the shock distance via the adjustment of the parameter $\bar{\beta}$: decreasing the value of $\bar{\beta}$ slows down the steepening process, so that shock wave formation takes place at a proportionally longer normalized propagation distance, as highlighted in Fig. 2. Conversely, along the time axis, the quasi-vertical front in the pulse trailing edge is always located at the same point for all three cases, regardless of the value of $\bar{\beta}$. In practice, in nonlinear optical fibers with Kerr coefficient γ, smaller values of $\bar{\beta}$ can be achieved by using either high peak powers P_0 or broader pulse durations T_0 of the input pulse. However, further control of TRP dynamics can be readily achieved by using different pulse shapes for the TRP initial amplitude profile. As an example, Fig. 3 illustrates the normalized longitudinal intensity evolution obtained for three different TRPs, i.e., generated from a hyperbolic secant, a finite-energy Airy, and a flat-top pulse (the amplitude profiles used for each case are provided in Table 1). For a relevant comparison, we performed numerical simulations under the same conditions as for the Gaussian TRP in Fig. 1 ($\bar{\beta} = 0.013$). In each case, we extracted the temporal intensity profiles at the shock distance of the Gaussian TRP, comparing the corresponding GNLSE profiles with analytical predictions from the IBE. While the Gaussian TRP exhibits the formation of a gradient catastrophe at Z = 30.63, the shock is observed at different locations for the other three cases. Basically, the smoothness of their amplitude profiles is responsible for different nonlinear evolutions. For instance, a flat-top TRP characterized by a steeper trailing edge displays an earlier shock formation, while the main lobe of an Airy TRP, owing to its smoother profile, tends to steepen later on during propagation.

Optics EXPRESS

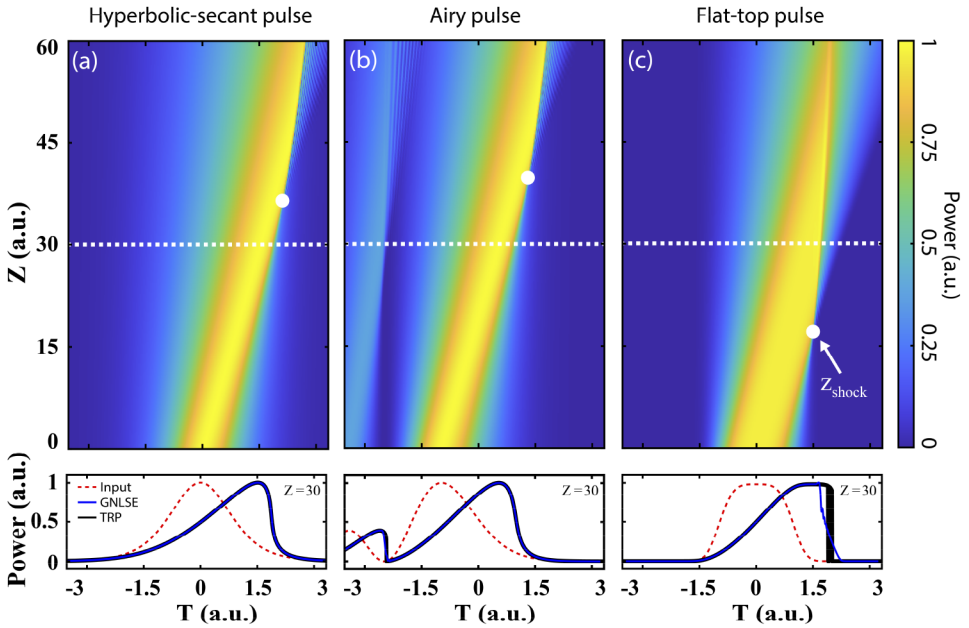

Fig. 3. Normalized longitudinal intensity evolution of TRPs from GNLSE simulations with $\tilde{\beta} = 0.013$, corresponding to different initial pulse amplitude profiles: (a) Hyperbolic secant pulse, (b) Airy pulse, and (c) Flat-top pulse. The white dots illustrate the shock locations for each TRP evolution, highlighting the effect produced by each initial envelope on the progressive pulse steepening. A TRP featuring a smoother input amplitude profile exhibits a shock formation occurring at a longer propagation distance (when compared, under the same propagation conditions, to a pulse with a steeper input amplitude profile). The lower panels illustrate the corresponding TRP numerical profiles (blue solid lines) at $Z = 30$ (corresponding to the shock distance of the Gaussian TRP in Fig. 1 - see dashed white lines), compared with analytical predictions (black solid lines). Red dashed lines mark the TRP initial profiles for each case.

Table 1. Amplitude profiles used for the study of TRPs with different initial shapes. The comparison among TRPs with different amplitude profiles is carried out by choosing the same scaling factor $T_0 = 4.95$ ps, for the pulse duration and $P_0 = 9.42$ W, for the peak power.

Third-order Riemann Pulse	Amplitude Profile
Gaussian	$\lvert A_{TRP}(T)\rvert = \exp(-T^2/2)$
Hyperbolic secant	$\lvert A_{TRP}(T)\rvert = \mathrm{sech}(T)$
Finite-energy Airy	$\lvert A_{TRP}(T)\rvert = 2.05\mathrm{Airy}(T)\exp(0.1T)$
Flat-top	$\lvert A_{TRP}(T)\rvert = \exp(-T^n/2)$ with $n = 4$

4. Third-order Riemann pulses under normal and anomalous group velocity dispersion

Now, we explore the dynamics of TRPs when their carrier wavelength moves away from the ZDW, so that their propagation is ruled by the mutual influence of both SOD and TOD. By assuming that only the parameter a in Eq. (6) is equal to 0 (i.e., the SOD coefficient is nonzero),

Optics EXPRESS

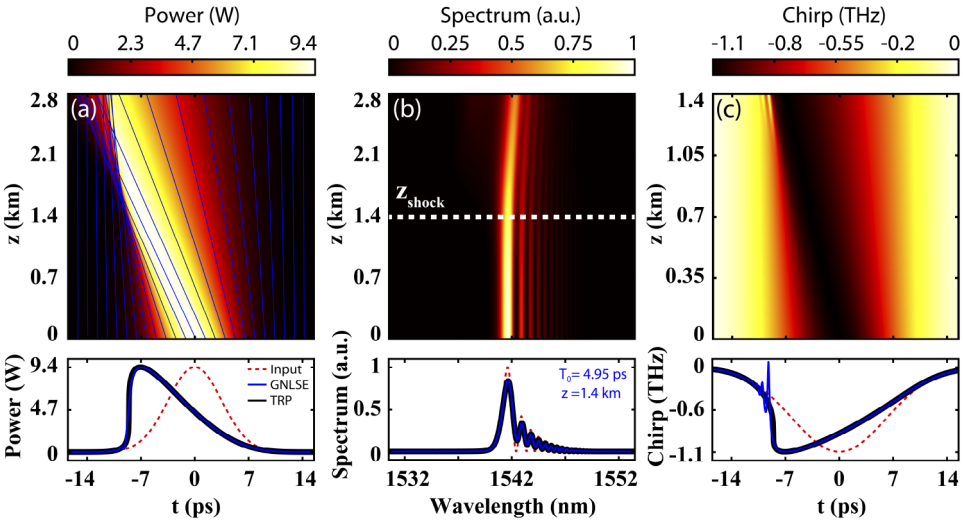

Fig. 4. GNLSE simulations showing the evolution of a Gaussian TRP over 2.8 km of dispersion-shifted fiber (DSF) at the ZDW and with pure negative TOD. Upper panels illustrate the longitudinal (a) power, (b) spectrum, and (c) chirp obtained from numerical simulations. Blue solid lines in (a) illustrate the characteristic lines from the IBE, while the white dotted line in (b) marks the shock distance. Lower panels show the corresponding profiles extracted at the shock distance along with analytical predictions from the IBE (black solid lines), and their initial profiles (red dashed lines).

the GNLSE system can be modelled in terms of a modified IBE:

$$\frac{\partial P}{\partial Z} + (P + \sigma)\frac{\partial P}{\partial T} = 0, \tag{10}$$

where $\sigma = -\ddot{\bar{\beta}}^2/(2\bar{\beta})$. Consequently, Eq. (7) with the inclusion of the SOD term acquires the form of shifted RWs [10]. Similar to the ZDW case, TRPs propagating under the mutual influence of SOD and TOD exhibit a progressive steepening as well as a subsequent shock wave formation, which is only determined by the parameter $\bar{\beta}$. Here, the SOD influence simply consists of imposing a transversal shift to the TRP along the time axis, thus enabling a control of the temporal position where the gradient catastrophe occurs. Specifically, the shock distance is only determined by the value of $\bar{\beta}$, while the shock time can be controlled by changing the parameter $\ddot{\bar{\beta}}$. Remarkably, the sign of the SOD coefficient has no influence on the additional temporal shift and TRPs can therefore be generated in both the normal and the anomalous dispersion regimes. This permits their existence even in the self-focusing regime of the GNLSE, where standard RWs are not permitted. In this regard, to better understand the physical origin of the TRP phenomenon behind the mathematical formalism, we have numerically tested the propagation of a TRP using the same propagation conditions (i.e., $\kappa = 0.104$) as a standard Riemann pulse in Ref. [7]. By artificially increasing over two-orders of magnitude the SOD coefficient (up to $M = 956$), we found that the peak intensity extracted at the shock distance varied less than 1 % compared to the ideal case of an input pulse injected at the fiber ZDW (i.e., with $M = 0$). In this section, we perform numerical simulations considering the realistic scenario of pulse propagation in a DSF. Here, TRPs with a Gaussian amplitude and negative chirp profiles are considered, but we note that other TRP conditions could also be readily excited. Numerical results, illustrated in Figs. 4 and 5, refer to the case of a Gaussian TRP, which propagates in 2.8 km-long DSF with and without the inclusion of either a normal or an anomalous GVD term. This is equivalent to selecting an

Optics EXPRESS

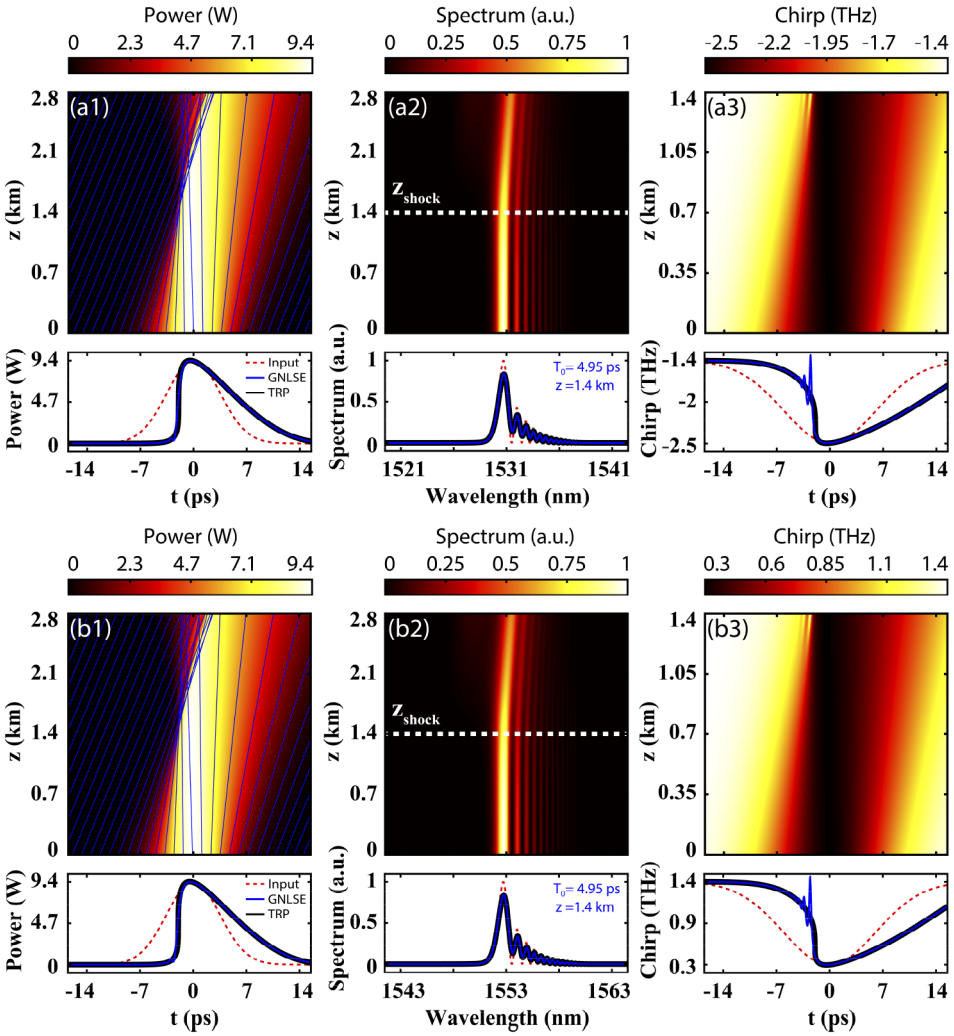

Fig. 5. GNLSE simulations of TRPs in a DSF with negative TOD and with either normal (upper TRP) or anomalous (lower TRP) GVD. Panel descriptions and parameters for both cases are the same as in Fig. 4, besides the values of β_2 being, for the upper and lower panels, 1.0793 and -1.0793 ps^2 km^{-1}, respectively.

optical fiber with both constant nonlinearity and GVD slope, while symmetrically shifting the ZDW location (or the excitation wavelength). Parameters used in simulations are $P_0 = 9.42$W, $T_0 = 4.95$ps, for the initial optical pulse, $\beta_2 = \pm 1.0793$ps^2 km^{-1}, $\beta_3 = -0.1234$ps^3 km^{-1}, and $\gamma = 0.5$W^{-1} km^{-1} for the DSF (at $\lambda_0 = 1550$ nm), which correspond to the normalized dispersion coefficients $\ddot{\beta} = \pm\, 0.097$ and $\bar{\beta} = -0.06$. The initial Gaussian amplitude, in dimensional units, is then defined as $|E_{TRP}(t, z = 0)| = \sqrt{P_0}\exp(t^2/2T_0^2)$. Noteworthy, under these conditions, is that a standard Riemann pulse cannot sustain the ideal evolution expected for RWs: the pulse would either undergo a continuous temporal broadening or compression of its envelope, depending on the sign of the GVD [38]. Differently, TRPs can maintain their typical Riemann dynamics. At the ZDW (see Fig. 4), shock wave formation occurs at the leading edge of the pulse after 1.4 km of propagation in the DSF, with a shock temporal coordinate T_{SC} estimated at -8.57 ps. The presence of the steepest front at the leading edge of the pulse is here simply induced by the

Optics EXPRESS

negative chirp [Fig. 4(c)]. Looking at the Fourier domain, the TRP spectrum (see Fig. 4(b)) exhibits an Airy-like shape, with a main lobe centered around $\lambda = 1542$ nm and a long tail stemming from the sub-lobes extending in the long-wavelength edge. For carrier wavelengths far from the ZDW, the effect of GVD is not negligible anymore. If the influence of TOD is small enough, a standard Riemann pulse can thus provide a good approximation of Riemann wave dynamics [7]. However, for higher TOD values (i.e., for decreasing M), the dynamics of the pulse evolution differ from a standard Riemann pulse: TRPs must be considered in this case. Moving away from the ZDW, and independently of the sign of the normalized SOD coefficient (i.e. for propagation occurring in either the normal or the anomalous dispersion regime), the TRPs evolution shown in Fig. 5 displays the same dynamics as those of Fig. 4, besides inducing an offset in the shock time T_{SC} (in that case being delayed to -1.97 ps). Characteristic lines calculated from Eq. (10) confirm the prediction for all cases under study, displaying an excellent match with GNLSE simulations. However, the influence of the GVD sign can be revealed by comparing the TRPs chirp and spectral profiles: For normal dispersion (i.e. $\beta_2 = 1.0793$ ps^2 km^{-1}), the TRP spectrum shifts towards lower wavelengths with respect to the ZDW case, with its main lobe being located at around $\lambda = 1531$ nm. In addition, the temporal chirp profile acquires a negative offset of -1.4 THz. Conversely, in the anomalous dispersion regime (i.e. $\beta_2 = -1.0793$ ps^2 km^{-1}), the TRP spectrum is shifted towards longer wavelengths, with a main lobe centered around $\lambda = 1553$ nm, and a positive offset of 1.4 THz for the pulse chirp. Note that, for the sake of clarity in this study, we have neglected Raman scattering effects in our GNLSE simulations. Such a delayed nonlinear response would in fact introduce a frequency shift during the pulse evolution and thus affect the TRP steepening dynamics that would slightly deviate from the ideal evolution described above. The impact of this Raman frequency shift is intrinsically linked to the initial pulse bandwidth (and its overlap with the Raman gain) as well as the propagation parameters. However, we have verified that the pulse evolution discrepancies are minimal and will not lead to any qualitative change. For instance, we found that the inclusion of Raman scattering (Raman fraction $f_R = 18$ %) in the simulations reported in Fig. 5 led to a marginal change in the pulse evolution, yielding a pulse peak power difference of only 0.04 % at the shock point when compared to the ideal TRPs.

5. Optical control of third-order Riemann pulses

It is known from the literature that a transversal (or temporal) control of the shock dynamics in standard RWs can be achieved by adding a linear phase term to the pre-designed temporal chirp [10], thus offering a certain degree of freedom on the wave steepening process. In contrast, for TRPs, both shock distance and time are uniquely determined by the choice of the carrier wavelength. As the latter is adjusted, new values for both the shock distance and time can be obtained. However, adding a linear phase term to the TRP does not allow to gain control over the shock time (as it is typically obtained for standard RWs), but it leads instead to a significant deterioration of the Riemann wave evolution. To govern TRPs propagation dynamics, a different approach must be implemented. In this last section, we describe a way to achieve such control by exploiting the a parameter of Eq. (7), whose adjustment allows for manipulating the nonlinear evolution of TRPs by acting on the temporal chirp profile. The introduction of a generalizes the class of TRPs: From a physical viewpoint, the parameter a brings a perturbation in the initial chirp profile induced by the addition of an artificial offset in the pulse amplitude used to calculate the TRP chirp in Eq. (5). This corresponds to introducing a background on the chirp profile as well as modifying its magnitude. Generalized TRPs still feature pulse steepening and a constant peak intensity evolution. However, the shock distance, time, and steepening direction can be significantly modified. In Fig. 6, in order to illustrate the influence of the parameter a, we carried out numerical simulations of Gaussian TRPs nonlinear evolution for the selected values. We use here the same parameters as in Fig. 4 but consider $\beta_3 = -0.001234$ ps^3 km^{-1} to provide a better

Optics EXPRESS

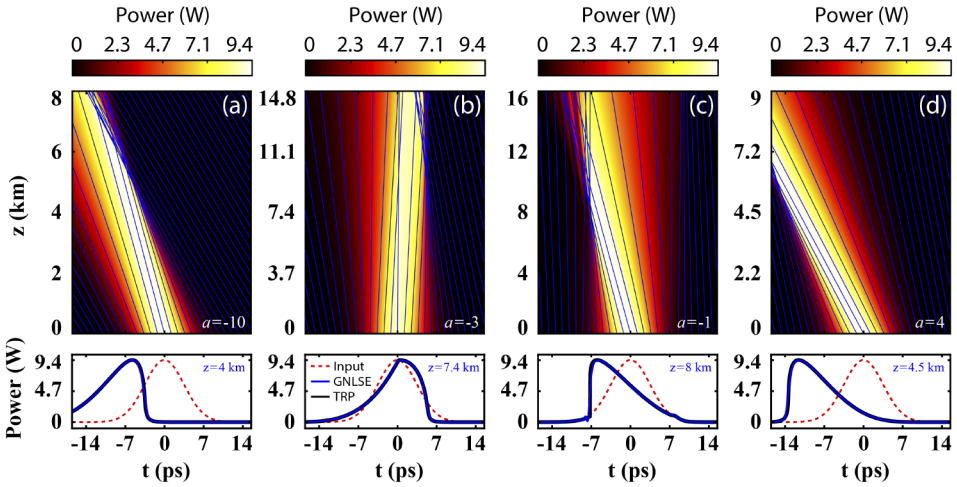

Fig. 6. GNLSE simulations of TRPs at the ZDW, with a pure negative TOD and for different values of the control parameter a: (a) $a = -10$, (b) $a = -3$, (c) $a = -1$, and (d) $a = 4$. Parameters used in simulations are the same as in Fig. 4, except for $\beta_3 = -0.001234$ ps^3 km^{-1} (or $\bar{\beta} = -0.013$). In the upper panels, blue solid lines overlapping each longitudinal intensity distribution represent characteristic lines calculated from the nonlinear wave equation in Eq. (6). Lower panels plot corresponding numerical intensity profiles (blue solid lines), extracted at the shock distance, along with analytical (black solid lines) and initial (red dashed lines) curves.

approximation of the Riemann wave evolution (i.e. using a smaller value of $\bar{\beta} = -0.013$ for a better NSWE-like approximation). We observe that, for small values of a, the behavior of the TRP is strongly nonlinear: the pulse envelope suffers a clear reshaping of its amplitude, which is eventually followed by pulse steepening, whose properties (e.g. edge side) can be controlled by adjusting a. Interestingly, we note that higher values of a lead to TRPs whose intensity profile resembles those of a simple Riemann pulse. The shock formation can take place either on the trailing or on the leading edge of the pulse, depending on the positive or negative sign of a, respectively. In this case, a can be employed as a control parameter of the TRP, with the potential to directly adjust both shock coordinates (i.e. time and distance). Once again, the characteristic lines calculated by Eq. (6) agree very well with numerical simulations for each case. Finally, it is worth mentioning that for very high values of a, the GNLSE evolution can be approximated reasonably well by a shifted TRP, according to the following expression, where Eq. (7) can be reduced as:

$$|A_{TRP}(T,Z)| \cong \left|A_{TRP}\left(T - 3\bar{\beta}a^{1/3}|A_{TRP}(T,Z)|Z - \left(\frac{\bar{\beta}}{2}a^{4/3} - \frac{\ddot{\beta}^2}{2\bar{\beta}}\right)Z\right)\right|. \tag{11}$$

Importantly, Eq. (11) provides a clear physical picture of the contribution brought by a on the dynamics of TRPs: This coefficient not only induces an additional shifting term connected to the SOD, but it is also responsible for the steepening process of the TRP, which for high values of a, is similar to the one occurring in a standard Riemann wave.

6. Conclusion

We have introduced the concept of TRPs in the context of nonlinear fiber optics and investigated analytically and numerically their properties under different propagation conditions. TRPs exist in the presence of both the TOD and the Kerr nonlinearity and can be generated in both

Optics EXPRESS

normal and anomalous group-velocity dispersion regimes, as well as exactly at the ZDW. During propagation, TRPs undergo a progressive steepening while maintaining a constant peak intensity, until they experience a shock wave formation. To control the TRP dynamics, we also introduced a phase-chirping control parameter a to adjust the initial chirp profile of the pulses. Under the same propagation conditions, diverse values of a induce different artificial backgrounds and amplitude rescaling on the initial TRPs chirp profile, thus generalizing the concept of TRPs to a broader class of nonlinear pulses. Remarkably, we have demonstrated that, for sufficiently high values of a, the pulse evolution can be well-approximated by a shifted TRP, where the shock properties (distance, time, and direction) can be controlled by acting on the values of a without the necessity to change the optical fiber parameters.

Funding

National Key Research and Development Program of China (2017YFA0303800); National Natural Science Foundation of China (11674180, 12022404, 62075105); Natural Sciences and Engineering Research Council of Canada; Canada Research Chairs; Higher Education Discipline Innovation Project (B07013); Ministère de l'Économie, de la Science et de l'Innovation - Québec; 66 Postdoctoral Science Grant of China; Mitacs (Globalink Research Award); Région Nouvelle-Aquitaine (Project SCIR); European Research Council (740355); Ministry of Education and Science of the Russian Federation (14.Y26.31.0017).

Acknowledgments

R.M. is affiliated to UESTC as an adjoint faculty.

Disclosures

The authors declare no conflicts of interest.

References

1. A. V. Gurevich, A. L. Krylov, and G. A. El, "Evolution of a Riemann wave in the dispersive hydrodynamics," Sov. Phys. JETP **74**(6), 957–962 (1992).
2. L. Francarollo and H. Capart, "Riemann wave description of erosional dam-break flows," J. Fluid Mech. **461**, 183–228 (2002).
3. W. Wan, S. Jia, and J. W. Fleischer, "Dispersive superfluid-like shock waves in nonlinear optics," Nat. Phys. **3**(1), 46–51 (2007).
4. S. Malaguti, A. Corli, and S. Trillo, "Control of gradient catastrophes developing from dark beams," Opt. Lett. **35**(24), 4217–4219 (2010).
5. N. Zahibo, E. Pelinovsky, T. Tapilova, and I. Nikolkina, "Savage-Hutter model for avalanche dynamics in inclined channels: Analytical solutions," J. Geophys. Res. **115**(B3), B03402 (2010).
6. I. Didenkulova and E. Pelinovsky, "Rogue waves in nonlinear hyperbolic systems (shallow-water framework)," Nonlinearity **24**(3), R1–R18 (2011).
7. B. Wetzel, D. Bongiovanni, M. Kues, Y. Hu, Z. Chen, S. Trillo, J. M. Dudley, S. Wabnitz, and R. Morandotti, "Experimental generation of Riemann waves in optics: a route to shock wave control," Phys. Rev. Lett. **117**(7), 073902 (2016).
8. S. Trillo and M. Conforti, "Shock Waves," in G.-D. Peng, (Eds.) *Handbook of Optical Fibers*, pp. 1–48, (Springer, 2017).
9. S. Randoux, F. Gustave, P. Suret, and G. A. El, "Optical random Riemann waves in integrable turbulence," Phys. Rev. Lett. **118**(23), 233901 (2017).
10. D. Bongiovanni, B. Wetzel, P. Yang, Y. Hu, Y. Qiu, J. Xu, S. Wabnitz, Z. Chen, and R. Morandotti, "Optical generation and control of spatial Riemann waves," Opt. Lett. **44**(14), 3542–3545 (2019).
11. G. Marcucci, D. Pierangeli, S. Gentilini, N. Ghofraniha, Z. Chen, and C. Conti, "Optical spatial shock waves in nonlocal nonlinear media," Adv. Phys.: X **4**(1), 1662733 (2019).
12. G. Marcucci, X. Hu, P. Cala, W. Man, D. Pierangeli, C. Conti, and Z. Chen, "Anisotropic optical shock waves in isotropic media with giant nonlocal nonlinearity," Phys. Rev. Lett. **125**, 243902 (2020).
13. Y. B. Zel'dovic, "Gravitational instability: An approximate theory for large density perturbations," Astron. Astrophys. **5**, 84–89 (1970).

Optics EXPRESS

14. M. A. Hoefer, M. J. Ablowitz, I. Coddington, E. A. Cornell, P. Engels, and V. Schweikhard, "Dispersive and classical shock waves in Bose-Einstein condensates and gas dynamics," Phys. Rev. A **74**(2), 023623 (2006).
15. S. Hodges and A. Carverhill, "Quasi-mean reversion in an efficient stock market; the characterization of economic equilibria which support Black-Scholes option pricing," Econom. J. **103**(417), 395–405 (1993).
16. D. Chowdhury, L. Santen, and A. Schadschneider, "Statistical physics of vehicular traffic and some related systems," Phys. Rep. **329**(4-6), 199–329 (2000).
17. M. J. Lighthill and G. B. Whitham, "On kinematic waves II. A theory of traffic flow on long crowded roads," Proc. R. Soc. Lond. A **229**(1178), 317–345 (1955).
18. C. M. Dafermos, *Hyperbolic Conservation Laws in Continuum Physics*, (Springer-Verlag, 2010).
19. G. P. Agrawal, *Nonlinear Fiber Optics* (5th edition), (Academic, 2012).
20. J. M. Dudley, G. Genty, and S. Coen, "Supercontinuum generation in photonic crystal fiber," Rev. Mod. Phys. **78**(4), 1135–1184 (2006).
21. S. Dyachenko, A. Newell, A. Pushkarev, and V. Zakharov, "Optical turbulence: weak turbulence, condensates and collapsing filaments in the nonlinear Schrödinger equation," Phys. D (Amsterdam, Neth.) **57**(1-2), 96–160 (1992).
22. C. Kharif, E. Pelinovsky, and A. Slunyaev, *Rogue Waves in the Ocean*, (Springer, 2009).
23. J. M. Dudley, F. Dias, M. Erkintalo, and G. Genty, "Instabilities, breathers and rogue waves in optics," Nat. Photonics **8**(10), 755–764 (2014).
24. D. R. Solli, C. Ropers, P. Koonath, and B. Jalali, "Optical rogue waves," Nature **450**(7172), 1054–1057 (2007).
25. T. B. Benjamin and J. E. Feir, "The disintegration of wave trains on deep water Part 1. Theory," J. Fluid Mech. **27**(3), 417–430 (1967).
26. N. Akhmediev and E. Pelinovsky, "Editorial–introductory remarks on "discussion & debate: Rogue waves–towards a unifying concept?" Eur. Phys. J. Spec. Top. **185**(1), 1–4 (2010).
27. C. Bonatto, M. Feyereisen, S. Barland, M. Giudici, C. Masoller, J. R. R. Leite, and J. R. Tredicce, "Deterministic optical rogue waves," Phys. Rev. Lett. **107**(5), 053901 (2011).
28. N. Akhmediev, J. M. Dudley, D. R. Solli, and S. K. Turitsyn, "Recent progress in investigating optical rogue waves," J. Opt. **15**(6), 060201 (2013).
29. M. Erkintalo, K. Hammani, B. Kibler, C. Finot, N. Akhmediev, J. M. Dudley, and G. Genty, "Higher-order modulation instability in nonlinear fiber optics," Phys. Rev. Lett. **107**(25), 253901 (2011).
30. J. M. Soto-Crespo, A. Ankiewicz, N. Devine, and N. Akhmediev, "Modulation instability, Cherenkov radiation, and Fermi–Pasta–Ulam recurrence," J. Opt. Soc. Am. B **29**(8), 1930–1936 (2012).
31. D. Solli, G. Herink, B. Jalali, and C. Ropers, "Fluctuations and correlations in modulation instability," Nat. Photonics **6**(7), 463–468 (2012).
32. S. Wabnitz, C. Finot, J. Fatome, and G. Millot, "Shallow water rogue wavetrains in nonlinear optical fibers," Phys. Lett. A **377**(12), 932–939 (2013).
33. B. Varlot, S. Wabnitz, J. Fatome, G. Millot, and C. Finot, "Experimental generation of optical flaticon pulses," Opt. Lett. **38**(19), 3899–3902 (2013).
34. G. B. Whitham, *Linear and Nonlinear Waves* (Wiley, 1974).
35. Y. Kodama and S. Wabnitz, "Analytical theory of guiding-center nonreturn-to-zero and return-to-zero signal transmission in normally dispersive nonlinear optical fibers," Opt. Lett. **20**(22), 2291–2293 (1995).
36. Y. Kodama, "The Whitham equations for optical communications: Mathematical theory of NRZ," SIAM J. Appl. Math. **59**(6), 2162–2192 (1999).
37. Y. Kodama, S. Wabnitz, and K. Tanaka, "Control of nonreturn-to-zero signal distortion by nonlinear gain," Opt. Lett. **21**(10), 719–721 (1996).
38. S. Wabnitz, "Optical tsunamis: shoaling of shallow water rogue waves in nonlinear fibers with normal dispersion," J. Opt. **15**(6), 064002 (2013).
39. J. Fatome, C. Finot, G. Millot, A. Armaroli, and S. Trillo, "Observation of optical undular bores in multiple four-wave mixing," Phys. Rev. X **4**(2), 021022 (2014).
40. G. Xu, M. Conforti, A. Kudlinski, A. Mussot, and S. Trillo, "Dispersive dam-break flow of a photon fluid," Phys. Rev. Lett. **118**(25), 254101 (2017).
41. G. Xu, D. Vocke, D. Faccio, J. Garnier, T. Roger, S. Trillo, and A. Picozzi, "From coherent shocklets to giant collective incoherent shock waves in nonlocal turbulent flows," Nat. Commun. **6**(1), 8131 (2015).
42. P. Sprenger, M. A. Hoefer, and G. A. El, "Hydrodynamic optical soliton tunneling," Phys. Rev. E **97**(3), 032218 (2018).